THE JOURNAL OF BIOLOGICAL CHEMISTRY VOL. 289, NO. 34, pp. 23723–23733, August 22, 2014


# The Conformational Changes Induced by Ubiquinone Binding in the $Na^+$-pumping NADH:Ubiquinone Oxidoreductase ($Na^+$-NQR) Are Kinetically Controlled by Conserved Glycines 140 and 141 of the NqrB Subunit*

Received for publication, April 16, 2014, and in revised form, July 8, 2014 Published, JBC Papers in Press, July 8, 2014, DOI 10.1074/jbc.M114.574640

**Madeleine Strickland[‡], Oscar Juárez[§], Yashvin Neehaul[‡1], Darcie A. Cook[§], Blanca Barquera[§2], and Petra Hellwig[‡3]**

*From the [‡]Laboratoire de Bioélectrochimie et Spectroscopie, UMR 7140, CNRS Université de Strasbourg, Strasbourg, France, 67000 and [§]Department of Biological Sciences, Center for Biotechnology and Interdisciplinary Studies, Rensselaer Polytechnic Institute, Troy, New York 12180*

**Background:** $Na^+$-pumping NADH:ubiquinone oxidoreductase ($Na^+$-NQR) is a respiratory enzyme which reduces ubiquinone.
**Results:** Two ubiquinone binding sites were found of which only one is catalytically relevant.
**Conclusion:** Gly-140/Gly-141 residues in the NqrB subunit control entry to the catalytic binding site.
**Significance:** Learning how conformational changes are linked to ubiquinone reduction is directly relevant to a large number of respiratory enzymes.

**$Na^+$-pumping NADH:ubiquinone oxidoreductase ($Na^+$-NQR) is responsible for maintaining a sodium gradient across the inner bacterial membrane. This respiratory enzyme, which couples sodium pumping to the electron transfer between NADH and ubiquinone, is not present in eukaryotes and as such could be a target for antibiotics. In this paper it is shown that the site of ubiquinone reduction is conformationally coupled to the NqrB subunit, which also hosts the final cofactor in the electron transport chain, riboflavin. Previous work showed that mutations in conserved NqrB glycine residues 140 and 141 affect ubiquinone reduction and the proper functioning of the sodium pump. Surprisingly, these mutants did not affect the dissociation constant of ubiquinone or its analog HQNO (2-*n*-heptyl-4-hydroxyquinoline *N*-oxide) from $Na^+$-NQR, which indicates that these residues do not participate directly in the ubiquinone binding site but probably control its accessibility. Indeed, redox-induced difference spectroscopy showed that these mutations prevented the conformational change involved in ubiquinone binding but did not modify the signals corresponding to bound ubiquinone. Moreover, data are presented that demonstrate the NqrA subunit is able to bind ubiquinone but with a low non-catalytically relevant affinity. It is also suggested that $Na^+$-NQR contains a single catalytic ubiquinone binding site and a second site that can bind ubiquinone but is not active.**

$Na^+$-pumping NADH:ubiquinone oxidoreductase ($Na^+$-NQR)[4] is a respiratory enzyme found in marine and pathogenic bacteria such as *Haemophilus influenzae* and *Vibrio cholerae* (1–3). $Na^+$-NQR obtains energy by oxidizing NADH and reducing ubiquinone, which allows it to maintain a sodium gradient across the inner bacterial membrane. The sodium gradient is used to sustain essential processes, including the transport of amino acids into the cell (4) and the rotation of flagella (5), but also helps the bacteria to live in highly salty environments, such as oceans and blood (1). $Na^+$-NQR is a source of unusual structural features containing riboflavin as a *bona fide* redox cofactor (6) and a conformationally driven sodium pumping mechanism that has not been found in any other respiratory enzyme. In addition it shares sequence similarities with only one other membrane-bound complex, the *Rhodobacter* nitrogen fixing protein (RNF), which is a sodium pumping ferredoxin:NADH dehydrogenase (7).

$Na^+$-NQR is an ~200-kDa integral membrane protein composed of six subunits (NqrA-F) (8, 9). Electron microscopy and x-ray crystallography provided low resolution structures of the $Na^+$-NQR complex (10) along with a 2.95 Å x-ray crystal structure of part of the NqrF subunit (PDB code 2R6H), which hosts NADH oxidation by flavin adenine dinucleotide (FAD) and subsequent electron transfer to a 2Fe-2S iron-sulfur cluster (11), and a 1.1 Å structure of *Parabacteroides distasonis* NqrC subunit (PDB code 3LWX), which lacks the covalently bound FMN cofactor. Although the structures of subunits NqrA, -B, -D, and -E remain to be elucidated, they have been intensively studied by diverse biophysical methods. NqrC and NqrB host the third and fourth steps of electron transfer via the covalently attached $FMN_C$ and $FMN_B$, respectively (12, 13). Finally, the

* This work was supported by the Institut Universitaire de France, the CNRS, the FRC-LABEX CSC and the Agence Nationale de la Recherche (to P. H. and M. S.) and National Science Foundation Grant MCB-1052234 (to B. B., O. J., and D. A. C.).

[1] Present address: Mauritius Oceanography Institute, Victoria Ave., France Center, Quatre Bornes, Mauritius.
[2] To whom correspondence may be addressed. Tel.: 1-518-276-3861; E-mail: barqub@rpi.edu.
[3] To whom correspondence may be addressed: Laboratoire de Bioélectrochimie et Spectroscopie, UMR 71401, rue Blaise Pascal, CNRS Université de Strasbourg, Strasbourg, France 67000. Tel.: 33-368-85-12-73; Fax: 33-368-85-16-62; E-mail: hellwig@unistra.fr.

[4] The abbreviations used are: $Na^+$-NQR, $Na^+$-NADH-ubiquinone oxidoreductase; HQNO, 2-*n*-heptyl-4-hydroxyquinoline *N*-oxide; CoQ-1/8, ubiquinone-1/8; DM, *n*-dodecyl-β-D-maltoside; LDAO, lauryldimethylamine *N*-oxide.

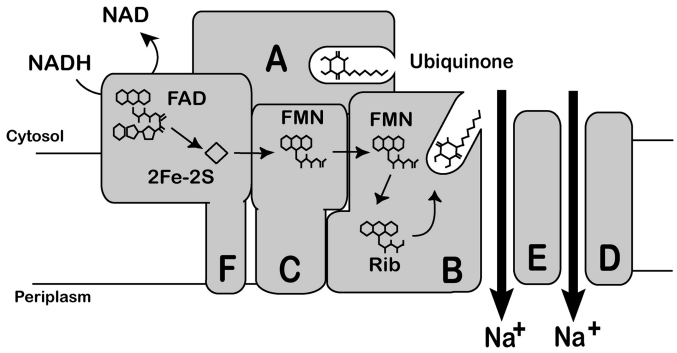


FIGURE 1. **Schematic view of the subunit and cofactor organization suggested for $Na^+$-NQR.** NADH is oxidized by FAD in subunit F. Electron transfer then occurs via 2Fe-2S (NqrF), $FMN_C$ (NqrC), $FMN_B$, and riboflavin (NqrB) to finally reduce the catalytic active ubiquinone to ubiquinol in NqrB. The picture shows a non-catalytically active quinone in NqrA. This process is coupled to sodium translocation across subunits NqrB, NqrD, and NqrE; see Ref. 19 and references therein for a more detailed discussion.

riboflavin resides in the NqrB subunit (9, 14) and reduces ubiquinone-8 ($Q_8$) to ubiquinol (15). NqrD and NqrE are contained entirely in the membrane and are responsible for sodium transfer via acidic amino acid side chains along with the NqrB subunit (16–18). A schematic view of the subunit and cofactor organization as currently discussed is presented in Fig. 1.

Different studies have addressed the identification of most ligand and cofactor binding sites in $Na^+$-NQR (9, 11–13). However, the exact localization of the ubiquinone binding site is not completely known. On the basis of studies involving a light-activated azido-quinone derivative 3-$N_3$-ubiquinone biotin, the inhibitor HQNO (2-*n*-heptyl-4-hydroxyquinoline *N*-oxide), and the analog dibromothymoquinone, it has been shown that the NqrA subunit is able to bind ubiquinone (20, 21). Indeed, HQNO binding prevents the reaction with the azido compound leading to the suggestion that the ubiquinone binding site might accommodate two ubiquinone molecules or one ubiquinone molecule and one inhibitor molecule (20, 21), as HQNO is a mixed-type inhibitor of $Na^+$-NQR with respect to ubiquinone and not a purely competitive inhibitor (22).

There is also evidence that a functional binding site for ubiquinone could be located in the membrane-bound NqrB subunit as a spontaneous mutation of glycine 141 (*V. cholerae* numbering), thought to be located on transmembrane helix III of NqrB, conferred resistance to HQNO (23). Subsequent functional characterization of NqrB-Gly-140 and NqrB-Gly-141 mutants led to the suggestion that Gly-141 is an important part of the ubiquinone binding site (24). However, Gly-140 seems to be much more important, as its mutation even to other small hydrophobic residues, such as alanine, completely abolished the apparent affinity of $Na^+$-NQR for ubiquinone ($K_m$) under steady state conditions (24).

To gain insight into the molecular mechanisms used by $Na^+$-NQR to bind ubiquinone and HQNO, further characterization of the mutants NqrB-G140A and NqrB-G141V was performed in this study together with the analysis of the ability of NqrA to bind ubiquinone and HQNO. Using a combination of mutagenesis, redox-dependent infrared spectroscopy, and equilibrium binding assays, it was found that the two conserved glycine residues do not participate directly in the ubiquinone binding site but control conformational changes that are involved in the capture of the substrate. We also discuss the low affinity ubiquinone binding to the NqrA subunit, which we found to be highly dependent on the presence of detergent, in contrast to the catalytically relevant ubiquinone binding site thought to be located in NqrB.

## EXPERIMENTAL PROCEDURES

The NqrB-G140A and NqrB-G141V mutants have been reported before (24). NqrA was cloned into the pBAD-HisA expression plasmid using the following primers: NQRAMED-HISTAG-FOR (atgcgaattcGAGGAATAATAAATGATTACA-ATAAAAAAGGGATTGGACCTTCCTATCGCAGGAA) and NQRAMEDHISTAG-REV (aagcttCTAATGGTGATGGTGAT-GATGACCTTCAAGCTCGCCCTTCCCTTCTTTCTCG). The construct included six amino acids (KGELEG) between the end of NqrA and a 6×-histidine tag. The proper construction of the plasmid was verified by DNA sequencing. The plasmid was introduced to the *nqr* deletion strain of *V. cholerae*.

*Cell Growth*—Recombinant Δ*nqr-V. cholerae* cells, containing wild-type $Na^+$-NQR (25), the mutants NqrB-G140A and NqrB-G141V (24), and the gene coding for NqrA, cloned into pBAD plasmids, were grown in LB medium at 37 °C. The cells were harvested, washed, and disrupted by passing the cells through a Microfluidizer at a pressure of 100 p.s.i. (25). The suspension was centrifuged for 10 h at 100,000 × *g* and in the case of wild-type $Na^+$-NQR and the mutants NqrB-G140A and NqrB-G141V, the cell membranes were recovered, washed, and used for purification as reported before (26). In the case of the NqrA subunit, the cytosolic fraction was used directly for protein purification as this subunit does not contain transmembrane domains.

*Protein Purification*—The cytosolic fraction containing NqrA (20–30 mg/ml) was incubated with nickel-nitrilotriacetic acid resin (0.5 ml nickel-nitrilotriacetic acid/ml of cytosolic fraction) for 30 min at 4 °C. The resin was packed into a column and washed with 5 volumes of buffer containing 5 mM imidazole, 50 mM $Na_2HPO_4$, 300 mM NaCl, 0.3% Triton X-100, 5 mM DTT, pH 8.0. The addition of DTT and detergent at this step was critical to avoid unspecific associations of proteins with NqrA or dimerization. A linear gradient of imidazole was applied from 50 to 500 mM, and a single peak containing an enriched fraction (50% of purity based on densitometry analysis of Coomassie Blue-stained SDS-PAGE) of NqrA was obtained at 270 mM imidazole. This fraction was diluted 20-fold, concentrated, and loaded onto an ion exchange DEAE column and washed with 4 volumes of buffer containing 50 mM Tris-HCl, 1 mM EDTA, 5% glycerol, 50 mM NaCl, pH 8.0. A gradient of 50–500 mM NaCl was applied, and a peak (at 350 mM NaCl) was recovered that contained a further enriched fraction of NqrA (70–80% purity). Finally, this fraction was collected, concentrated, and subjected to gel filtration chromatography. After three purification steps, the final relative concentration of $Na^+$-NQR in the samples was >92%.

*Activity Measurements*—Wild-type $Na^+$-NQR activity was measured as reported previously (14) by following spectrophotometrically the reduction of ubiquinone and the oxidation of NADH at 282 and 340 nm, respectively.

**TABLE 1**

**Dissociation constants for ubiquinone-1 and HQNO from wild-type $Na^+$-NQR and the mutants NqrB-G140A and NqrB-G141V and the isolated NqrA subunit before and after a wash with LDAO**

The NqrA subunit was also studied in varying quantities of the detergent DM. Full-length wild-type, NqrB-G140A, and NqrB-G141V complexes were studied in the presence of 0.05% DM.

| | Dissociation constants | | | | | |
|---|---|---|---|---|---|---|
| | Ubiquinone-1 | | | HQNO | | |
| Protein | $K_{D1}$ | $K_{D1}$[a] | $K_{D2}$[a] | $K_{D1}$ | $K_{D1}$[a] | $K_{D2}$[a] |
| | | | $\mu M$ | | | |
| Wild type | 10.5 ± 2.6 | 12.6 ± 5.6 | 0.16 ± 0.05 | 0.4 ± 0.04 | 0.51 ± 0.09 | 0.02 ± 0.008 |
| NqrB-G140A | 11.3 ± 3.5 | 8.6 ± 3.7 | 0.15 ± 0.05 | 0.4 ± 0.05 | 0.37 ± 0.08 | 0.018 ± 0.007 |
| NqrB-G141V | 9.6 ± 1.6 | 10.7 ± 4.2 | 0.14 ± 0.04 | 1.4 ± 0.16 | 1.7 ± 0.08 | 0.014 ± 0.005 |
| NqrA | 50.3 ± 14 | 47.4 ± 16 | | 69.5 ± 11 | | |
| NqrA + 0.02% DM | 120.4 ± 26 | | | | | |
| NqrA + 0.05% DM | 216.5 ± 57 | | | 280 ± 63 | | |

[a] Proteins listed in these columns underwent an LDAO wash.

*$K_D$ Measurements*—The dissociation constants for ubiquinone-1 (CoQ-1) and HQNO from $Na^+$-NQR were measured by equilibrium dialysis. 100 $\mu$l of the protein samples at a concentration of 50 $\mu$M were loaded into Pierce 96-well microdialysis devices (10-kDa molecular weight cut off membrane). The dialysis samples were incubated for 12 h in equilibration buffer containing CoQ-1 or HQNO (100 $\mu$M). The content of CoQ-1 and HQNO was measured spectrophotometrically at 282 and 346 nm, respectively, using molar extinction coefficients of 14.85 and 9.6 $mM^{-1}$ $cm^{-1}$.

*Infrared Spectroscopy*—Wild-type $Na^+$-NQR and the NqrB-G140A and NqrB-G141V mutants were exchanged into 50 mM sodium phosphate, 150 mM NaCl, 0.05% *n*-dodecyl-$\beta$-D-maltoside (DM) at pH 8 before infrared experiments. CoQ-1 or HQNO were dissolved in ethanol and dried with mediators (28) before protein was added at a 1:1 molar ratio (usually around 600 $\mu$M). Mediators accelerated electron transfer but did not contribute to the spectrum due to their low final concentration (31 $\mu$M). The mixture was incubated on ice for 20 min before assembling the electrochemical cell. The electrochemically induced FTIR difference spectra were obtained using a three-electrode electrochemical cell with optically transparent $CaF_2$ windows as described previously (29). To avoid protein adsorption to the working electrode, the gold grid was modified with an aqueous solution containing cysteamine (1 mM) and mercaptopropionic acid (1 mM) for at least 1 h. The infrared spectra were recorded on a Vertex 70 FTIR spectrometer (Bruker) using a spectral range of 4000–1000 $cm^{-1}$. Reduction and oxidation of the enzyme were studied using a potential step of −620 to +200 mV (*versus* $Ag^+$/AgCl; add +208 mV for standard hydrogen electrode). Spectra were then recorded after an equilibration time of 2 and 4 min for oxidation and reduction, respectively. For each step two spectra (256 scans and 4 $cm^{-1}$ resolution) were recorded and averaged. The reaction was typically cycled 50–60 times, and the difference spectra were averaged. The temperature of the electrochemical cell was fixed at 5 °C throughout the experiment. Infrared spectra were humidity and base-line-corrected, and double difference spectra were obtained by normalization and interactive subtraction.

## RESULTS

*Affinity of Wild-type $Na^+$-NQR, Glycine Mutants, and the NqrA Subunit for Ubiquinone*—To characterize the effects of the conserved glycine residue mutants, the dissociation constants ($K_D$) for ubiquinone-1 and HQNO from $Na^+$-NQR were measured (Table 1, Fig. 2). The binding experiments were performed in wild-type $Na^+$-NQR, NqrB-G140A, and NqrB-G141V mutants and in the isolated NqrA subunit. The binding was analyzed in the protein preparation after purification, as described under "Experimental Procedures," and also after a wash with 0.05% LDAO. $Na^+$-NQR was reported to contain a tightly bound ubiquinone in substoichiometric ratios (~0.6 mol of CoQ per mol of $Na^+$-NQR), which can be eliminated in the presence of LDAO (30). The effect of LDAO (a zwitterionic detergent) and $\beta$-D-dodecyl maltoside (a nonionic detergent) on the $Na^+$-NQR activity was studied. It was reported that dodecyl-maltoside, a mild detergent, produced a fully active enzyme, but the addition of LDAO partially inactivated the enzyme activity and stripped the tightly bound ubiquinone from the enzyme (30). Casutt *et al.* (21) proposed that the azido quinone compound could be labeling the quinone binding site occupied by the tightly bound ubiquinone. Moreover, Nedielkov *et al.* (20) proposed that this binding site might accommodate up to two ubiquinone molecules.

Data shown in Fig. 2 and Table 1 indicate that wild-type $Na^+$-NQR and the mutants NqrB-G140A and NqrB-G141V are all able to bind only one ubiquinone molecule and one HQNO molecule. However, after washing the preparations with LDAO, which eliminates the tightly bound ubiquinone (20, 21), the three proteins were able to bind two ubiquinone molecules, of which one site has a high affinity for both ubiquinone and HQNO (Table 1). On the other hand, our data also show that the NqrA subunit is also able to bind one CoQ or one HQNO molecule. The $K_D$ for ubiquinone in NqrA is much higher than the $K_D$ for ubiquinone of the $Na^+$-NQR complex, at 50.3 $\mu$M, which is too high to actually participate in the catalytic cycle of the enzyme. The affinity for ubiquinone in NqrA is further reduced by moderately increasing the detergent concentration, and with 0.05% of DM (a concentration used in activity assays) the $K_D$ becomes 216.5 $\mu$M, which is completely out of the physiological range. In contrast with previous studies that suggested that NqrA could bind two ubiquinone molecules (20, 21), we observe that this subunit only binds one. This difference may be based on the different experimental techniques used (20, 21).

Importantly it can be shown that the mutants NqrB-G140A and NqrB-G141V have no major effect on the affinity of the

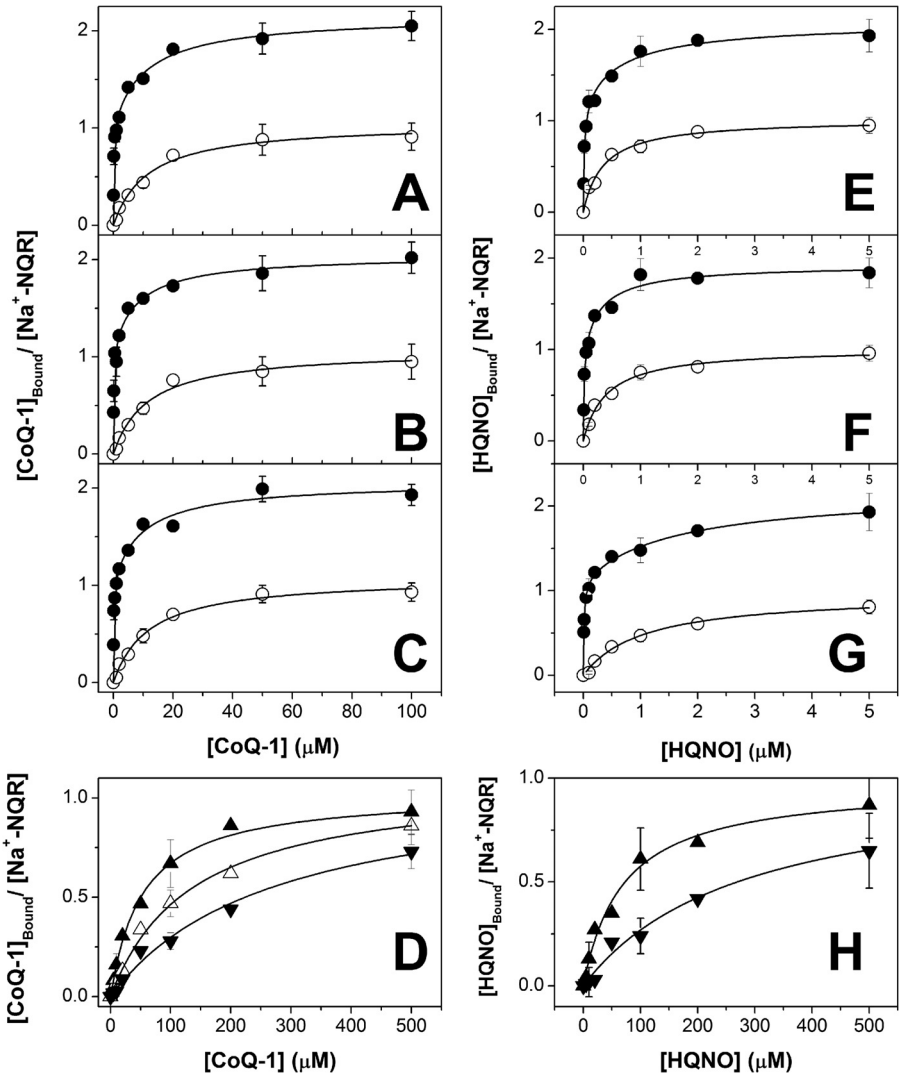


FIGURE 2. **Binding of CoQ-1 and HQNO to wild-type $Na^+$-NQR, NqrB-G140A, and NqrB-G141V mutant $Na^+$-NQR, and the NqrA subunit.** The binding experiments were performed by equilibrium dialysis after 12 h of incubation with buffer containing different concentrations of the ligands, as described under "Experimental Procedures." *Insets A*, *B*, *C*, and *D* show the amount of CoQ-1 bound per mol of the wild-type $Na^+$-NQR, NqrB-G140A, NqrB-G141V, and NqrA, respectively. *Insets E*, *F*, *G*, and *H* show the amount of HQNO bound per mol of the wild-type $Na^+$-NQR, NqrB-G140A, NqrB-G141V, and NqrA, respectively. The binding of HQNO and CoQ-1 to wild-type $Na^+$-NQR, NqrB-G140A, and NqrB-G141V (*insets A*, *B*, *C*, *E*, *F*, and *G*) was assayed in the proteins as obtained after two purification steps (○) or after a wash with LDAO (●), which eliminates the tightly bound ubiquinone-8. In the case of NqrA (*insets D* and *H*) the binding was assayed in the absence (▲) or in the presence of 0.02% (△) or 0.05% (▼) of DM.

enzyme for ubiquinone, as $K_D$ values close to wild-type $Na^+$-NQR can be found at around 10 $\mu$M. This is surprising because both mutations largely increased the $K_{m(app)}$ of the enzyme under steady-state conditions (24). The NqrB-G140A mutant produced the largest change, showing an unsaturable behavior for ubiquinone. Also, the rate of reduction of this mutant with ubiquinol was 2 orders of magnitude smaller with respect to wild-type $Na^+$-NQR, an indication that the binding site for the substrate might be disrupted in this mutant. Taking these results together, it is evident that the mutations in the NqrB subunit affect the reduction rate of ubiquinone but not the binding affinity ($K_D$). Thus, these glycine residues likely control the entry of ubiquinone to its binding site rather than participate directly in ubiquinone binding, which would explain the kinetic effect of the mutants. It is also important to point out that the $K_m$ value was considerably lower with respect to the $K_D$ (2.5 $\mu$M *versus* 10.5 $\mu$M) (24).

*Functional Characterization of the Ubiquinone Binding Sites*—According to the evidence shown in this work, the enzyme is active with one binding site but contains another site with high affinity for ubiquinone. As mentioned before, there is controversy regarding the number of functional binding sites in the enzyme. To clarify the role of the two ubiquinone binding sites in the catalytic mechanism of $Na^+$-NQR, a functional characterization of the enzyme was performed in the presence of different concentrations of ubiquinone and HQNO.

Fig. 3 shows the model that we used to fit and simulate the data. The sections of the model colored in black describe the binding of one ubiquinone molecule to the enzyme and its reduction to form ubiquinol, with the kinetic constants $k_{cat1}$ and $K_m$. According to our hypothesis, this simple scheme should be able to explain the behavior of the enzyme as isolated after two purification steps containing only one accessible ubiquinone binding site. The data were also fitted using a model

in which the enzyme would contain two catalytic binding sites, as proposed previously (20, 21). The model explaining this behavior includes the main central steps (Fig. 3, *black*) and the *blue section*, which contains the binding of another ubiquinone molecule with the apparent dissociation constant from Na$^+$-NQR of $Kr_Q$. One of the predictions of this model is that the enzyme should only be catalytically active after the two ubiquinone binding sites are occupied, thus $k_{cat1} = 0$; in other words the binding of the ubiquinone molecules will be sequential.

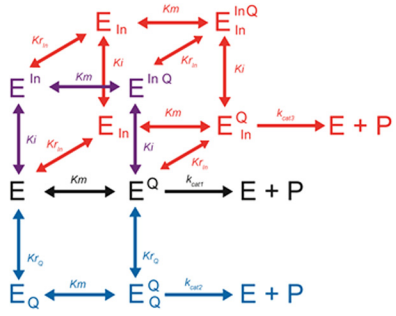


FIGURE 3. **Kinetic model of the interactions of ubiquinone (*Q*) and HQNO (*In*) with Na$^+$-NQR (*E*) during the catalytic cycle.** The *black part of the scheme* describes the binding of CoQ to the enzyme and the reduction to ubiquinol, which follows a Michaelis-Menten behavior. The enzyme can also contain a separate binding site for CoQ (shown in *blue*), which may contribute to the catalytic mechanism of the enzyme; thus, it does not modify the $K_m$ or $k_{cat}$. The model also includes the type of inhibition exerted by HQNO, which is non-competitive, binding to the free form of the enzyme ($E^{In}$) and to the form that contains CoQ ($E^{In\ Q}$). According to our data, the wash with LDAO would remove the tightly bound CoQ-8, which would allow the enzyme to bind HQNO and CoQ-1, both, to the catalytic site and to the high affinity site. In particular the enzyme would be able to bind a HQNO molecule in the high affinity site and CoQ-1 in the catalytic binding site ($E^{Q}_{In}$), producing a form that will be fully functional ($k_{cat1} = k_{cat3} = k_{cat2}$).

The two models described were then compared with the fit of the saturation kinetics of the enzyme (Fig. 4). We noticed that the model for a single catalytic ubiquinone binding site was able to fit the data. The two-ubiquinone-binding site model did not produce a good fit because it predicted a strong negative cooperativity, which is not observed experimentally. Also the simulation of the behavior using the affinity constants obtained by Casutt *et al.* (21) produced a line that did not describe the behavior from the experimental points, especially when comparing the predictions of the double reciprocal plot (*inset*, Fig. 4).

To further characterize the system, the same experiments were also performed in the enzyme washed with LDAO, in which the two ubiquinone binding sites could be accessible to the added ubiquinone (21). Thus, the enzyme would be able to bind two ubiquinone molecules, one in the catalytic site and one more in the high affinity site, represented in the blue and black sections of the model. The main difference of the single site model with the two-binding site-model prediction is that in the first case the enzyme should be functional with one or two ubiquinone molecules bound, $k_{cat1} = k_{cat2}$. The data were fitted to this model, and a $K_m$ value was obtained for the one catalytic binding site model, very close to the value obtained before (4.2 $\mu$M). The binding constant for the high affinity site is close to the $K_{D2}$ obtained under equilibrium conditions ($K$rQ = 0.02 $\mu$M) (Table 1).

Finally, the experiments were also performed in the presence of the inhibitor HQNO, which is a non-competitive inhibitor against quinone and has a strong effect over the $k_{cat}$ of the enzyme but no effects over the $K_m$ (24). The model that predicts

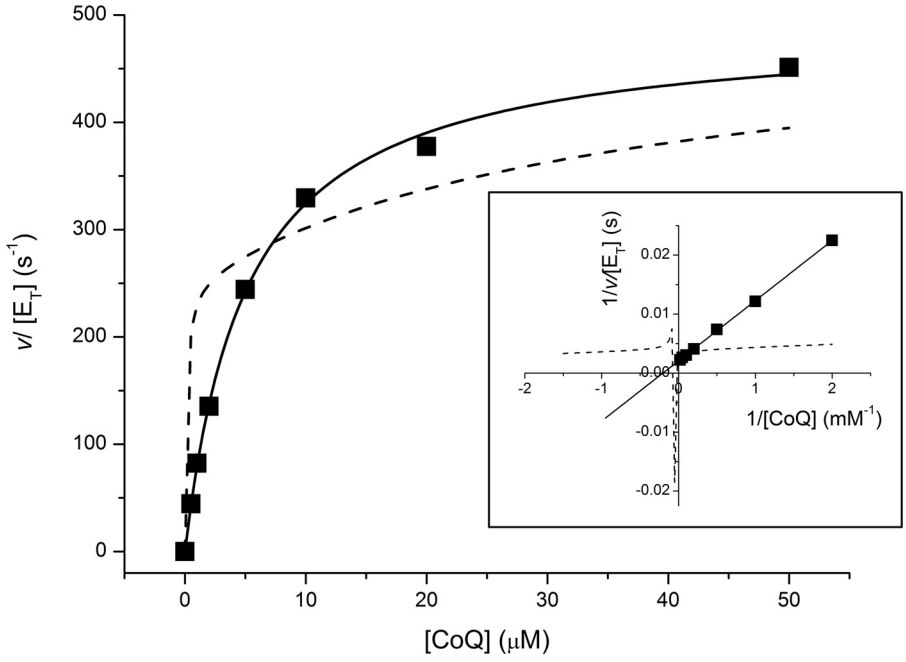


FIGURE 4. **Saturation kinetics of wild-type Na$^+$-NQR for CoQ-1.** The activity of Na$^+$-NQR was assayed spectrophotometrically, as described under "Experimental Procedures," using different concentrations of CoQ-1. The data were fitted using the equations obtained from Fig. 3 (*solid line*), considering that the enzyme contains only one catalytic binding site ($K_m$ = 3.9 $\mu$M) and a high affinity site ($Kr_Q$ = 0.02 $\mu$M) that can bind CoQ-1 but does not participate in catalysis ($k_{cat1} = k_{cat2}$). The model that considers two active catalytic sites was unable to fit the data, producing strong negative cooperativity behavior. The data obtained by Casutt *et al.* (21) were used to simulate the behavior of the complex using the apparent dissociation constants of CoQ-1 obtained by this group for NqrA (*dashed line*). It is evident that the two catalytic binding sites model are unable to explain the behavior of the enzyme, which is made clearer by comparing the predictions of the two models in the double reciprocal plot (*inset*).

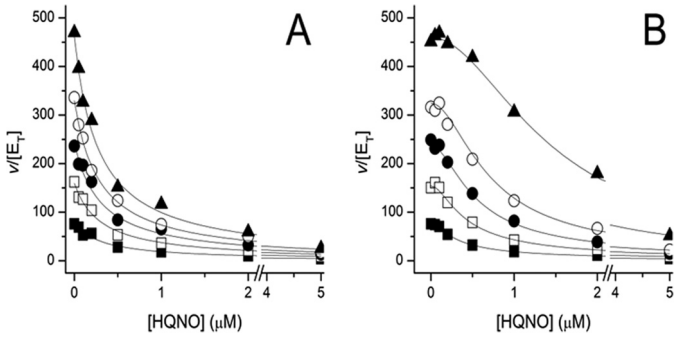


FIGURE 5. **Inhibition of wild-type $Na^+$-NQR by HQNO.** The CoQ-1 reductase activity of the enzyme was assayed at several fixed concentrations of the substrate, CoQ-1: 1 μM (■), 2 μM (□), 5 μM (●), 10 μM (○), and 50 μM (▲). The experiments were carried out using the enzyme as obtained after two purification steps (*A*) and after a wash with LDAO (*B*). The enzyme was diluted 20-fold with buffer containing 0.1% LDAO, concentrated to 1 ml, diluted 20-fold again, and re-concentrated. No changes in activity were evident after the two washing steps.

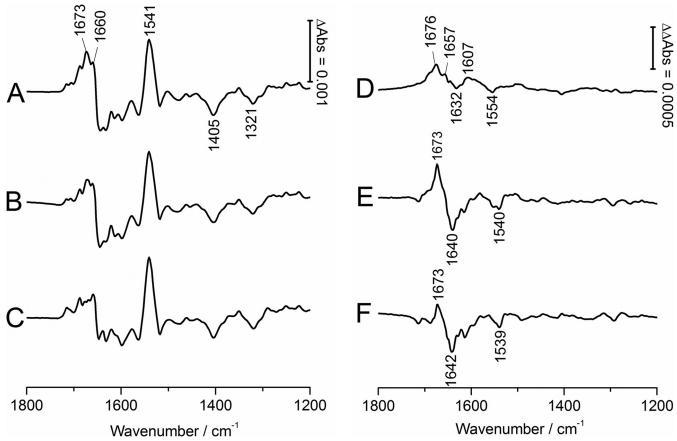


FIGURE 6. Shown are oxidized-minus-reduced FTIR difference spectra of the wild-type $Na^+$-NQR (*A*), the NqrB-G140A mutant (*B*), and the NqrB-G141V mutant (*C*) for the potential step between −620 and +200 mV. WT-minus-G140A (*D*), WT-minus-NqrB-G141V (*E*), and NqrB-G140A-minus-NqrB-G141V (*F*) double difference spectra were obtained by interactive subtraction. Peaks are summarized in Table 2.

this inhibition behavior is the purple part of the scheme, with the inhibition constant $K_i$. In the enzyme washed with LDAO, it is expected that the high affinity site would also participate in the mechanism of the enzyme, forming ternary complexes with the enzyme containing ubiquinone and HQNO (red section of the model). One of the most important differences in the single *versus* the double catalytic ubiquinone binding site models is the inhibition by HQNO. According to the predictions of the two-ubiquinone-binding site model, the wash with LDAO should not affect the inhibition pattern by HQNO. In contrast, under the single binding site model, the wash with LDAO would significantly change the mechanism of inhibition of HQNO. In fact, the binding of the inhibitor to the high affinity site would prevent inhibition in the catalytic site because the population of the enzyme would move toward productive forms ($E^{Q}_{IN}$) (Fig. 3). Data shown in Fig. 5 compare the inhibition obtained by HQNO at different CoQ-1 concentrations in the enzyme before (*A*) and after (*B*) the LDAO wash. It is evident that the enzyme after the LDAO wash shows a certain resistance to low HQNO concentrations, as predicted by the model. These data confirm that the high affinity site does participate in catalysis as demonstrated extensively in this work and other studies (15, 25, 31–35). In addition the data indicate that although the enzyme contains two potential ubiquinone binding sites, only one is catalytically active.

*FTIR Difference Spectra of Wild-type $Na^+$-NQR, NqrB-G140A, and NqrB-G141V Mutant Enzymes*—Electrochemically induced difference spectroscopy allows the observation of spectral changes in a studied molecule upon applying a potential. Proteins that contain redox cofactors can be studied by electrochemically induced UV-visible spectroscopy by placing the enzyme inside an optically transparent electrochemical cell (29). Alterations in the potential can yield spectra of the protein in the fully or partially reduced or oxidized state; thus, the technique is capable of studying one or more cofactors (36). $Na^+$-NQR from *V. cholerae* has been studied using this method, and past experiments involve investigation of the mid-point potentials of the redox cofactors (24, 25) and mutagenesis to study the sodium translocation mechanism (16). The electrochemical cell can also be used in combination with infrared spectroscopy. This technique allows the monitoring of changes of conformation or the protonation state of individual amino acids, the peptide backbone, flavins, or bound quinones. In this paper the two mutants NqrB-G140A and NqrB-G141V are compared with wild-type $Na^+$-NQR in the presence of ubiquinone-1 or HQNO to study redox-induced conformational changes upon binding to substrate or inhibitor.

The fully oxidized-minus-fully reduced (+200 mV minus −620 mV) FTIR difference spectra for wild-type and NqrB-G140A and NqrB-G141V mutant $Na^+$-NQR are presented in Fig. 6, *A–C*, respectively. The spectral region 1800–1200 $cm^{-1}$ is shown because it contains information on conformational changes in the backbone of the protein, the flavin cofactors, ubiquinone, and amino acid side chains while omitting contributions from the phosphate buffer that occur below 1200 $cm^{-1}$. Fe-S contributions from the iron-sulfur cluster are expected at even lower spectral frequencies (37). Key spectral features that confirm the presence of redox-active flavins include the large positive peak at 1541 $cm^{-1}$ due to a redox-induced change in the $\nu$(C═C) stretch, the large negative peak at 1405 $cm^{-1}$, which shows coupled $\delta(C\text{-}H)^{in\text{-}plane}/\delta(N\text{-}H)^{in\text{-}plane}$ bending, and the fingerprint of positive and negative peaks in the amide I region between 1600 and 1700 $cm^{-1}$ (peaks and attributions are summarized in Table 2) (38).

In the region 1500–1200 $cm^{-1}$, the NqrB-G140A difference spectrum (Fig. 6*B*) is very similar to wild-type $Na^+$-NQR (Fig. 6*A*), where the majority of intense peaks are due to flavins (1541, 1405, and 1321 $cm^{-1}$). This suggests that the mutation has not caused a large alteration in the environments of the four flavin cofactors. Moreover, we have previously demonstrated that the midpoint potentials of the different cofactors remain unaltered in the NqrB-G140A mutant, which causes the more drastic changes in the activity of the enzyme (24). We have also demonstrated, by following the amide-I band in the mid-infrared absorption spectra of the mutants, that the general structure of the enzyme is not altered in comparison to the wild-type enzyme.

**TABLE 2**

**Peaks from the oxidized-minus-reduced FTIR difference spectra of the wild-type $Na^+$-NQR (WT), the NqrB-G140A mutant, and the NqrB-G141V mutant for the potential step between −620 and +200 mV in the absence or presence of 1:1 ubiquinone-1**

Peaks shown are in units of wavenumber ($cm^{-1}$) and are described as positive (+) or negative (−). Spectra obtained on the absence (−Q) and presence (+Q) of CoQ-1 are displayed in Figs. 6, *A–C* and 7, *A–C*, respectively.

| WT (-Q) | WT (+Q) | NqrB-G140A (-Q) | NqrB-G140A (+Q) | NqrB-G141V (-Q) | NqrB-G141V (+Q) | Tentative assignments |
|---|---|---|---|---|---|---|
| **1715 (+)** | 1715 (+) | 1715 (+) | 1715 (+) | 1715 (+) | 1715 (+) | $\nu(C_4{=}O)$ of flavins, $\nu$(C=O) of Asp/Glu |
| **1706 (+)** | 1706 (+) | 1707 (+) | 1706 (+) | 1707 (+) | 1708 (+) | $\nu(C_4{=}O)$ of flavins, $\nu$(C=O) of Asp/Glu |
| **1687 (+)** | 1687 (+) | 1687 (+) | 1687 (+) | 1688 (+) | 1687 (+) | Amide I ($\beta$-turn), $\nu(C_2{=}O)$ of flavins |
| **1673 (+)** | 1671 (+) | 1672 (+) | 1672 (+) | 1677 (+) | 1668 (+) | Amide I ($\beta$-turn), $\nu(C_2{=}O)$ of flavins, $\nu$(C=O) of quinone, $\nu$(C=O) of Asn/Gln, $\nu_{as}(CN_3H_5^+)$ of Arg |
| **1660 (+)** | 1661 (+) | 1660 (+) | 1660 (+) | 1659 (+) | 1660 (+) | Amide I ($\alpha$-helix), $\nu$(C=O) of flavins, $\nu$(C=O) of quinone |
| **1644 (-)** | 1646 (-) | 1644 (-) | 1645 (-) | 1648 (-) | 1645 (-) | Amide I (random coil), $\nu(C_4{=}O)$ of flavins |
| **1632 (-)** | 1631 (-) | 1633 (-) | 1632 (-) | 1632 (-) | 1633 (-) | Amide I ($\beta$-sheet), $\nu(C_4{=}O)$ of flavins, $\nu_s(CN_3H_5^+)$ of Arg |
| **1614 (-)** | 1615 (-) | 1613 (-) | 1614 (-) | 1611 (-) | 1614 (-) | Amide I ($\beta$-sheet), $\nu$(C=N) of flavins, $\nu$(C=C) of quinone, $\delta(NH_2)$ of Asn/Gln, Tyr ring |
| **1598 (-)** | 1597 (-) | 1598 (-) | 1597 (-) | 1599 (-) | 1597 (-) | $\nu(C_{4a}{=}C_{10a})$ of flavins, $\nu$(C=C) of quinone, $\nu_{as}(COO^-)$ of Asp/Glu, Tyr ring |
| **1563 (-)** | 1562 (-) | 1564 (-) | 1563 (-) | 1563 (-) | 1563 (-) | Amide II, $\nu(C_{10a}{=}N_1)$, $\nu(C_{4a}{=}N_5)$ of flavins, $\nu_{as}(COO^-)$ of Asp/Glu |
| **1541 (+)** | 1540 (+) | 1541 (+) | 1541 (+) | 1541 (+) | 1541 (+) | Amide II, $\nu$(C=C) of neutral flavins, $\nu_{as}(COO^-)$ of Asp/Glu, $\delta_s(NH_3^+)$ of Lys |
| **1518 (-)** | 1518 (-) | 1518 (-) | 1518 (-) | 1518 (-) | 1518 (-) | $\delta(C_6\text{-H})$, $\delta(C_9\text{-H})$, $\delta(N_5\text{-H})$, $\delta(N_1\text{-H})$ of flavins, Tyr ring |
| **1478 (-)** | 1474 (-) | 1481 (-) | 1475 (-) | 1477 (-) | 1474 (-) | $\delta_{as}(C\text{-}H_3)$, quinone ring reorganization, $\delta_{as}(C\text{-}H_3)$ |
| **1454 (-)** | 1454 (-) | 1454 (-) | 1455 (-) | 1450 (-) | 1454 (-) | $\delta(C\text{-}H_2)$ |
| | 1430 (-) | | 1428 (-) | | 1429 (-) | Quinone ring reorganization |
| **1405 (-)** | 1403 (-) | 1405 (-) | 1404 (-) | 1405 (-) | 1403 (-) | $\delta(C\text{-}H)^{in\text{-}plane}/\delta(N\text{-}H)^{in\text{-}plane}$ of flavins, $\nu_s(COO^-)$ of Asp/Glu |
| **1350 (+)** | 1350 (+) | 1350 (+) | 1351 (+) | 1351 (+) | 1351 (+) | Isoalloxazine ring reorganization |
| **1337 (-)** | 1337 (-) | 1337 (-) | 1336 (-) | 1338 (-) | 1338 (-) | Isoalloxazine ring reorganization, $\delta$(C-H) |
| **1321 (-)** | 1321 (-) | 1321 (-) | 1321 (-) | 1320 (-) | 1320 (-) | Isoalloxazine ring reorganization, $\delta$(C-H) |
| **1304 (-)** | 1304 (-) | 1305 (-) | 1304 (-) | 1304 (-) | 1304 (-) | Isoalloxazine ring reorganization, $\delta$(C-H) |
| | 1289 (+) | | 1289 (+) | | 1288 (+) | C-$OCH_3$ of quinone |
| | 1265 (+) | | 1265 (+) | | 1265 (+) | C-$OCH_3$ of quinone |
| | 1205 (+) | | 1204 (+) | | 1204 (+) | Quinone |

In the amide I and II spectral region (1700–1540 $cm^{-1}$), which is also sensitive to conformational change, to ubiquinone, and amino acid side-chain contributions (39–42), only very small changes are seen when comparing wild-type and mutant enzymes. To highlight these changes, a double difference spectrum was calculated (Fig. 6*A* minus Fig. 6*B*: WT minus G140A) and is displayed in Fig. 6*D*. For example, the large positive peak at 1676 $cm^{-1}$ in Fig. 6*D* describes a decrease of the intensity of the peak at 1673 $cm^{-1}$ upon mutation from wild-type to NqrB-G140A. This decrease in amplitude could be due to a restriction in conformational flexibility in response to the mutation to a less flexible residue. However, $\nu$(C═O) ubiquinone peaks are also expected to fall in the region of 1660–1670 $cm^{-1}$ (40). In this region there are two peaks that could contain contributions from ubiquinone in the wild-type spectrum (Fig. 6*A*): at 1660 and 1673 $cm^{-1}$. These two peaks could describe two ubiquinone molecules bound to wild-type $Na^+$-NQR, or alternatively, they could contain contributions from only one ubiquinone molecule where the two carbonyl groups are bound in a different manner, splitting the signal into

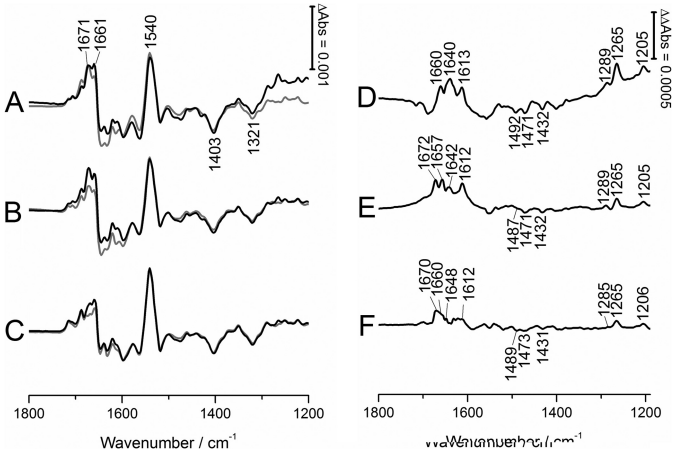


FIGURE 7. Shown are oxidized-minus-reduced FTIR difference spectra of the wild-type $Na^+$-NQR (*A*), the NqrB-G140A mutant (*B*), and the NqrB-G141V mutant (*C*) in the presence of ubiquinone-1 (1:1 protein to CoQ-1 molar ratio) for the potential step between −620 and +200 mV. WT, NqrB-G140A, and NqrB-G141V spectra from Fig. 6 are shown in *gray* for comparison, overlaid with *A*, *B*, and *C*, respectively. WT with CoQ-1-minus-WT (*D*), NqrB-G140A with CoQ-1-minus-NqrB-G140A (*E*), and NqrB-G141V with CoQ-1-minus-NqrB-G141V double difference spectra were obtained by interactive subtraction. Peaks are summarized in Table 2.

two parts (40). In either case the positive peaks in the WT-minus-G140A double difference spectrum at 1676 and 1657 $cm^{-1}$ could represent a reduction in the quantity of bound ubiquinone in the NqrB-G140A mutant. However, there is no difference in other peaks previously established to correspond to ubiquinone, such as 1288 and 1265 $cm^{-1}$ (40). Thus the data might indicate that the redox-driven conformational changes in these mutants are altered in comparison to wild-type $Na^+$-NQR.

Furthermore, in the double difference spectrum of WT-minus-NqrB-G141V (Fig. 6*E*), there is a clear positive peak at 1673 $cm^{-1}$ which indicates that the NqrB-G141V mutant is also different from the wild-type, but crucially, to a larger extent than NqrB-G140A as the amplitude of this signal is increased. This could indicate that the much larger valine residue could restrict conformational change still further.

*FTIR Difference Spectra in the Presence of CoQ-1*—Ubiquinone-8 (CoQ-8) is predicted to bind in the NqrB subunit of $Na^+$-NQR because it accepts electrons from riboflavin (15); therefore, the interaction of ubiquinone with the wild type and NqrB-G140A and NqrB-G141V mutants was studied. It is not practical to use CoQ-8 in experiments due to its low solubility in aqueous solution; therefore, CoQ-1 was used as a functional substitute.

The fully oxidized-minus-fully reduced FTIR difference spectra for wild-type, NqrB-G140A, and NqrB-G141V $Na^+$-NQR in the presence of CoQ-1 (1:1 ratio) are shown in Fig. 7, *A*–*C*, with assignments in Table 2. The corresponding spectra in the absence of CoQ-1 are displayed in *gray*. Previously, similar experiments were carried out for the photosynthetic reaction center (41) and cytochrome $bo_3$ (40) in the presence of ubiquinone; therefore, modes corresponding to ubiquinone are well known and can be assigned. Unbound ubiquinone in aqueous solution is known to have a broad positive peak at 1652 $cm^{-1}$ with a shoulder at 1664 $cm^{-1}$ in the oxidized-minus-reduced difference spectra that is due to a redox-induced change in the $\nu$(C═O) stretch. However, in the bound form of ubiquinone this peak becomes narrower due to the restriction in flexibility imposed by the binding pocket. In addition, the signal may shift upon binding.

In the double difference spectrum of WT with CoQ-1-minus-WT (Fig. 7*D*), contributions from bound ubiquinone can be seen. The narrow $\nu$(C═O) band at 1660 $cm^{-1}$ can be tentatively assigned to the C═O group of the bound ubiquinone in wild-type $Na^+$-NQR. For NqrB-G140A, however, this band appears at a lower wave number (1657 $cm^{-1}$), suggesting that the ubiquinone environment is different for the mutant. When comparing the ubiquinone double difference spectra of wild type and NqrB-G140A (Fig. 7, *D* and *E*, respectively), a new positive peak appears at 1672 $cm^{-1}$ for NqrB-G140A that is completely absent in wild-type $Na^+$-NQR. This new band could indicate that the ubiquinone carbonyls in the NqrB-G140A binding site undergo splitting. Perturbations in the binding site could decrease the strength of one carbonyl bond in the bound ubiquinone while increasing the strength of the other. This is not unsurprising, as the mutant reduces ubiquinone less well (24). Further quinone signals are found for the $\nu$(C═C) mode at 1613 $cm^{-1}$ and at 1289 and 1265 $cm^{-1}$ for the signals from the C-$OCH_3$ vibrations of the 2- and the 3-methoxy groups. The ring modes of the fully reduced and protonated forms of ubiquinol contribute with negative bands at 1492, 1471, and 1432 $cm^{-1}$ (40).

The NqrB-G141V mutant enzyme also presents two peaks in the ubiquinone binding region of the double difference spectrum, with the main peak at 1670 and a shoulder at 1660 $cm^{-1}$ (Fig. 7*F*). Alternatively, the new peaks at 1673 and 1670 $cm^{-1}$ for NqrB-G140A and NqrB-G141V, respectively, could indicate a perturbation in a flavin carbonyl or indeed conformational coupling to ubiquinone. However, this is highly unlikely, as vibrational modes in the flavin are highly coupled, and no further flavin signals are perturbed.

Because the mutations do not affect binding affinity ($K_D$), but do affect activity of the enzyme (24), this could indicate an indirect role for glycines 140 and 141 in ubiquinone reduction. The residues may not be part of the catalytic site but could be involved in a vestibule that controls the passage of ubiquinone to the binding site, thus exclusively affecting the kinetic parameters of the mutants ($K_m$) but not the thermodynamic properties of the binding site ($K_D$).

*FTIR Difference Spectra in the Presence of HQNO*—HQNO and korormicin are non-competitive inhibitors of ubiquinone binding in $Na^+$-NQR (22, 43). Korormicin is predicted to bind near the NqrB-Gly-141 residue as spontaneous *Vibrio alginolyticus* NqrB-G141V mutants (*V. cholerae* numbering) were found to be resistant to the antibiotic (23). Because HQNO and korormicin compete for the same binding site, it was concluded that HQNO binding occurs near to this residue.

HQNO binding was investigated by the addition of a 1:1 molar ratio to wild-type $Na^+$-NQR and the NqrB-G140A and NqrB-G141V mutants for which the redox-induced infrared difference spectra are shown in Fig. 8 (*traces A*, *B*, and *C*, respectively). Double difference spectra were also produced and are shown in Fig. 8, *traces D–F*. Key features of HQNO binding to

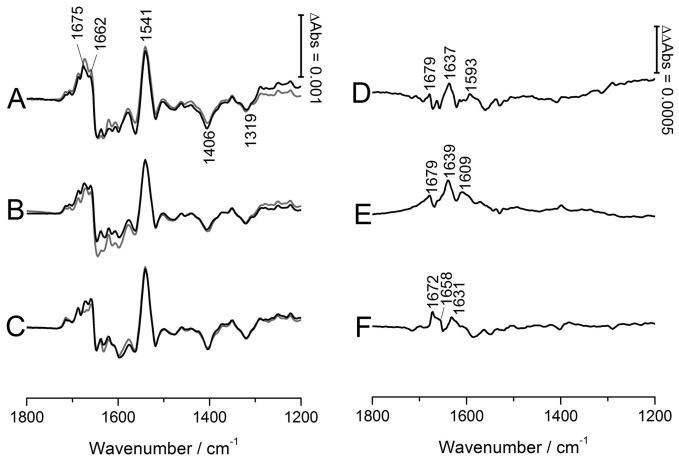


FIGURE 8. Shown are oxidized-minus-reduced FTIR difference spectra of the wild-type $Na^+$-NQR (*A*), the NqrB-G140A mutant (*B*), and the NqrB-G141V mutant (*C*) in the presence of HQNO (1:1 molar ratio) for the potential step between −620 and +200 mV. WT, NqrB-G140A, and NqrB-G141V spectra from Fig. 6 are shown in *gray* for comparison, overlaid with A, B and C, respectively. WT with HQNO-minus-WT (*D*), NqrB-G140A with HQNO-minus-NqrB-G140A (*E*), and NqrB-G141V with HQNO-minus-NqrB-G141V (*F*) double difference spectra obtained by interactive subtraction.

wild-type $Na^+$-NQR (Fig. 8*D*) include positive peaks at 1679 and 1637 $cm^{-1}$. These peaks could be associated either with the HQNO molecule itself or with conformational changes within the protein caused by the binding of HQNO. In the double difference spectrum for the NqrB-G140A mutant (Fig. 8*E*), these peaks were found at 1679 and 1639 $cm^{-1}$, which indicates that the NqrB-G140A mutant binds to HQNO in a similar mode as wild type. However, the positive peak at 1593 $cm^{-1}$ in wild-type $Na^+$-NQR was shifted to 1609 $cm^{-1}$ in the NqrB-G140A mutant, indicating that there is some perturbation to the binding site.

For the NqrB-G141V mutant, which is largely insensitive to the inhibitor, the three peaks in this region were 1672, 1658, and 1631 $cm^{-1}$, revealing additional conformational changes in the protein in the mutant and thus a clear change of the HQNO binding site in the NqrB-G141V mutant enzyme in comparison to both wild-type and NqrB-G140A. This would confirm that the HQNO binding site is located at or near the NqrB-G141V residue, as previously suggested (23, 24). Interestingly, because the ubiquinone binding site may not be located near to this residue, HQNO inhibition could be carried out via long range conformational blocking of the protein, preventing ubiquinone reduction. This certainly tallies with the non-competitive nature of HQNO inhibition in $Na^+$-NQR.

## DISCUSSION

$Na^+$-NQR couples sodium pumping to ubiquinone reduction. We previously suggested that the mechanism of sodium translocation by $Na^+$-NQR involves conformational changes that are responsible for the capture of sodium on one side of the membrane and its release on the opposite side. Indeed, with the use of IR spectroscopy we have been able to establish that wild-type $Na^+$-NQR undergoes large conformational changes and in the backbone of the protein itself upon reduction and oxidation, which facilitates sodium pumping (16). The two mutations we have investigated reduce or abolish ubiquinone reduction (NqrB-G141V and NqrB-G140A, respectively (24)) but do not alter the affinity of ubiquinone for $Na^+$-NQR as shown in this report. Ubiquinone binding experiments showed that NqrA binds CoQ-1 only very weakly, whereas the $K_D$ is diminished beyond physiologically relevant levels upon the addition of the detergent DM. Thus the results clarify the role of NqrB-Gly-140 and NqrB-Gly-141 in the catalytic binding site of ubiquinone and also suggest that the site in NqrA could be nonspecific and probably related to the exposure of hydrophobic cavities in the isolated subunit that are not accessible in the full $Na^+$-NQR complex. It may thus not participate in the catalytic cycle of the enzyme.

It cannot be excluded, however, that a larger binding site is present, as discussed for example for the respiratory complex I, where different types of inhibitors have been found to bind to one long and narrow site (27, 44). Also, a large hydrophobic cavity including more than one subunit needs to be kept in mind. The mutants studied would in this case be part of the regulatory mechanism. Within these lines the electrochemically induced infrared difference spectra showed that the two mutants have a lower amplitude in the amide I region, and therefore, the conformational change seen in wild-type $Na^+$-NQR is partially blocked. NqrB-G140A and NqrB-G141V mutants behaved differently in comparison to wild-type $Na^+$-NQR upon the addition of ubiquinone, which indicates that the mutations altered ubiquinone reduction in some way. This difference could be due to the conformational coupling between the ubiquinone binding site and the NqrB-Gly-140 and NqrB-Gly-141 residues discussed above. Similar experiments in the presence of HQNO showed that the binding mode for the NqrB-G141V mutant with this inhibitor is significantly perturbed. On the other hand, this perturbation is lessened for the NqrB-G140A mutant, indicating that the HQNO binding site is closer to the Gly-141 residue. It is, therefore, suggested that the HQNO binding site might include residue NqrB-Gly-141 and is conformationally coupled to the true catalytic ubiquinone binding site, which is also located in NqrB.

## REFERENCES

1. Hayashi, M., Nakayama, Y., and Unemoto, T. (1996) Existence of $Na^+$-translocating NADH-quinone reductase in *Haemophilus influenzae*. *FEBS Lett.* **381,** 174–176
2. Tokuda, H., and Unemoto, T. (1982) Characterization of the respiration-dependent $Na^+$ pump in the marine bacterium *Vibrio alginolyticus*. *J. Biol. Chem.* **257,** 10007–10014
3. Häse, C. C., and Mekalanos, J. J. (1999) Effects of changes in membrane sodium flux on virulence gene expression in *Vibrio cholerae*. *Proc. Natl. Acad. Sci. U.S.A.* **96,** 3183–3187
4. Unemoto, T., Akagawa, A., and Hayashi, M. (1993) Correlation between the respiration-driven $Na^+$ pump and the $Na^+$-dependent amino acid transport in moderately halophilic bacteria. *J. Gen. Microbiol.* **139,** 2779–2782
5. Dibrov, P. A., Kostryko, V. A., Lazarova, R. L., Skulachev, V. P., and Smirnova, I. A. (1986) The sodium cycle. I. $Na^+$-dependent motility and modes of membrane energization in the marine alkalotolerant *Vibrio alginolyticus*. *Biochim. Biophys. Acta* **850,** 449–457
6. Barquera, B., Zhou, W., Morgan, J. E., and Gennis, R. B. (2002) Riboflavin is a component of the $Na^+$-pumping NADH-quinone oxidoreductase from *Vibrio cholerae*. *Proc. Natl. Acad. Sci. U.S.A.* **99,** 10322–10324
7. Jouanneau, Y., Jeong, H. S., Hugo, N., Meyer, C., and Willison, J. C. (1998) Overexpression in *Escherichia coli* of the *rnf* genes from *Rhodobacter cap-*

*sulatus.* Characterization of two membrane-bound iron-sulfur proteins. *Eur. J. Biochem.* **251,** 54–64
8. Rich, P. R., Meunier, B., and Ward, F. B. (1995) Predicted structure and possible ionmotive mechanism of the sodium-linked NADH-ubiquinone oxidoreductase of *Vibrio alginolyticus*. *FEBS Lett.* **375,** 5–10
9. Casutt, M. S., Huber, T., Brunisholz, R., Tao, M., Fritz, G., and Steuber, J. (2010) Localization and function of the membrane-bound riboflavin in the $Na^+$-translocating NADH:quinone oxidoreductase ($Na^+$-NQR) from *Vibrio cholerae*. *J. Biol. Chem.* **285,** 27088–27099
10. Lunin, V. Y., Lunina, N. L., Casutt, M. S., Knoops, K., Schaffitzel, C., Steuber, J., Fritz, G., and Baumstark, M. W. (2012) Low-resolution structure determination of $Na^+$-translocating NADH:ubiquinone oxidoreductase from *Vibrio cholerae* by *ab initio* phasing and electron microscopy. *Acta Crystallogr. D Biol. Crystallogr.* **68,** 724–731
11. Barquera, B., Nilges, M. J., Morgan, J. E., Ramirez-Silva, L., Zhou, W., and Gennis, R. B. (2004) Mutagenesis study of the 2Fe-2S center and the FAD binding site of the $Na^+$-translocating NADH:ubiquinone oxidoreductase from *Vibrio cholerae*. *Biochemistry* **43,** 12322–12330
12. Barquera, B., Häse, C. C., and Gennis, R. B. (2001) Expression and mutagensis of the NqrC subunit of the NQR respiratory $Na^+$ pump from *Vibrio cholerae* with covalently attached FMN. *FEBS Lett.* **492,** 45–49
13. Hayashi, M., Nakayama, Y., Yasui, M., Maeda, M., Furuishi, K., and Unemoto, T. (2001) FMN is covalently attached to a threonine residue in the NqrB and NqrC subunits of $Na^=$-translocating NADH-quinone reductase from *Vibrio alginolyticus*. *FEBS Lett.* **488,** 5–8
14. Juárez, O., Nilges, M. J., Gillespie, P., Cotton, J., and Barquera, B. (2008) Riboflavin is an active redox cofactor in the $Na^+$-pumping NADH:quinone oxidoreductase ($Na^+$-NQR) from *Vibrio cholerae*. *J. Biol. Chem.* **283,** 33162–33167
15. Juárez, O., Morgan, J. E., and Barquera, B. (2009) The electron transfer pathway of the $Na^+$-pumping NADH:quinone oxidoreductase from *Vibrio cholerae*. *J. Biol. Chem.* **284,** 8963–8972
16. Neehaul, Y., Juárez, O., Barquera, B., and Hellwig, P. (2013) Infrared spectroscopic evidence of a redox-dependent conformational change involving ion binding residue NqrB-D397 in the $Na^+$-pumping NADH:quinone oxidoreductase from *Vibrio cholerae*. *Biochemistry* **52,** 3085–3093
17. Shea, M. E., Juárez, O., Cho, J., and Barquera, B. (2013) Aspartic acid 397 in subunit B of the $Na^+$-pumping NADH:quinone oxidoreductase from *Vibrio cholerae* forms part of a sodium binding site, is involved in cation selectivity, and affects cation binding site cooperativity. *J. Biol. Chem.* **288,** 31241–31249
18. Juárez, O., Athearn, K., Gillespie, P., and Barquera, B. (2009) Acid residues in the transmembrane helices of the $Na^+$-pumping NADH:quinone oxidoreductase from *Vibrio cholerae* involved in sodium translocation. *Biochemistry* **48,** 9516–9524
19. Juárez, O., and Barquera, B. (2012) Insights into the mechanism of electron transfer and sodium translocation of the $Na^+$-pumping NADH:quinone oxidoreductase. *Biochim. Biophys. Acta* **1817,** 1823–1832
20. Nedielkov, R., Steffen, W., Steuber, J., and Möller, H. M. (2013) NMR reveals double occupancy of quinone-type ligands in the catalytic quinone binding site of the $Na^+$-translocating NADH:quinone oxidoreductase from *Vibrio cholerae*. *J. Biol. Chem.* **288,** 30597–30606
21. Casutt, M. S., Nedielkov, R., Wendelspiess, S., Vossler, S., Gerken, U., Murai, M., Miyoshi, H., Möller, H. M., and Steuber, J. (2011) Localization of ubiquinone-8 in the $Na^+$-pumping NADH:quinone oxidoreductase from *Vibrio cholerae*. *J. Biol. Chem.* **286,** 40075–40082
22. Nakayama, Y., Hayashi, M., Yoshikawa, K., Mochida, K., and Unemoto, T. (1999) Inhibitor studies of a new antibiotic, korormicin, 2-*n*-heptyl-4-hydroxyquinoline *N*-oxide and $Ag^+$ toward the $Na^+$-translocating NADH-quinone reductase from the marine *Vibrio alginolyticus*. *Biol. Pharm. Bull.* **22,** 1064–1067
23. Hayashi, M., Shibata, N., Nakayama, Y., Yoshikawa, K., and Unemoto, T. (2002) Korormicin insensitivity in *Vibrio alginolyticus* is correlated with a single point mutation of Gly-140 in the NqrB subunit of the $Na^+$-translocating NADH-quinone reductase. *Arch. Biochem. Biophys.* **401,** 173–177
24. Juárez, O., Neehaul, Y., Turk, E., Chahboun, N., DeMicco, J. M., Hellwig, P., and Barquera, B. (2012) The role of glycine residues 140 and 141 of subunit B in the functional ubiquinone binding site of the $Na^+$-pumping NADH:quinone oxidoreductase from *Vibrio cholerae*. *J. Biol. Chem.* **287,** 25678–25685
25. Neehaul, Y., Juárez, O., Barquera, B., and Hellwig, P. (2012) Thermodynamic contribution to the regulation of electron transfer in the $Na^+$-pumping NADH:quinone oxidoreductase from *Vibrio cholerae*. *Biochemistry* **51,** 4072–4077
26. Juárez, O., Shea, M. E., Makhatadze, G. I., and Barquera, B. (2011) The role and specificity of the catalytic and regulatory cation-binding sites of the $Na^+$-pumping NADH:quinone oxidoreductase from *Vibrio cholerae*. *J. Biol. Chem.* **286,** 26383–26390
27. Baradaran, R., Berrisford, J. M., Minhas, G. S., Sazanov, L. A. (2013) Crystal structure of the entire respiratory complex I. *Nature* **494,** 443–448
28. Hellwig, P., Scheide, D., Bungert, S., Mäntele, W., and Friedrich, T. (2000) FT-IR spectroscopic characterization of NADH:ubiquinone oxidoreductase (Complex I) from *Escherichia coli*: oxidation of FeS cluster N2 is coupled with the protonation of an aspartate or glutamate side chain. *Biochemistry* **39,** 10884–10891
29. Moss, D., Nabedryk, E., Breton, J., and Mäntele, W. (1990) Redox-linked conformational changes in proteins detected by a combination of infrared spectroscopy and protein electrochemistry. *Eur. J. Biochem.* **187,** 565–572
30. Barquera, B., Hellwig, P., Zhou, W., Morgan, J. E., Häse, C. C., Gosink, K. K., Nilges, M., Bruesehoff, P. J., Roth, A., Lancaster, C. R., and Gennis, R. B. (2002) Purification and characterization of the recombinant $Na^+$-translocating NADH:quinone oxidoreductase from *Vibrio cholerae*. *Biochemistry* **41,** 3781–3789
31. Bogachev, A. V., Kulik, L. V., Bloch, D. A., Bertsova, Y. V., Fadeeva, M. S., and Verkhovsky, M. I. (2009) Redox properties of the prosthetic groups of $Na^+$-translocating NADH:quinone oxidoreductase. 1. Electron paramagnetic resonance study of the enzyme. *Biochemistry* **48,** 6291–6298
32. Bogachev, A. V., Bloch, D. A., Bertsova, Y. V., and Verkhovsky, M. I. (2009) Redox properties of the prosthetic groups of $Na^+$-translocating NADH:quinone oxidoreductase. 2. Study of the enzyme by optical spectroscopy. *Biochemistry* **48,** 6299–6304
33. Bogachev, A. V., Bertsova, Y. V., Ruuge, E. K., Wikström, M., and Verkhovsky, M. I. (2002) Kinetics of the spectral changes during reduction of the $Na^+$-motive NADH:quinone oxidoreductase from. *Vibrio harveyi*. *Biochim. Biophys. Acta* **1556,** 113–120
34. Barquera, B., Ramirez-Silva, L., Morgan, J. E., and Nilges, M. J. (2006) A new flavin radical signal in the $Na^+$-pumping NADH:quinone oxidoreductase from *Vibrio cholerae*: an EPR/electron nuclear double resonance investigation of the role of the covalently bound flavins in subunits B and C. *J. Biol. Chem.* **281,** 36482–36491
35. Barquera, B., Morgan, J. E., Lukoyanov, D., Scholes, C. P., Gennis, R. B., and Nilges, M. J. (2003) X- and W-band EPR and Q-band ENDOR studies of the flavin radical in the $Na^+$-translocating NADH:quinone oxidoreductase from *Vibrio cholerae*. *J. Am. Chem. Soc.* **125,** 265–275
36. Hellwig, P., and Melin, F. (2010) Recent applications of infrared spectroscopy and microscopy in chemistry, biology, and medicine. In *Handbook of Porphyrin Science with Applications to Chemistry, Physics, Materials Science, Engineering, biology, and Medicine, Vol. 7: Physicochemical characterization*, pp. 462–473, World Scientific Publishing Co. Pte. Ltd., Singapore
37. El Khoury, Y., and Hellwig, P. (2011) A combined far-infrared spectroscopic and electrochemical approach for the study of iron-sulfur proteins. *Chemphyschem* **12,** 2669–2674
38. Wille, G., Ritter, M., Friedemann, R., Mäntele, W., and Hübner, G. (2003) Redox-triggered FTIR difference spectra of FAD in aqueous solution and bound to flavoproteins. *Biochemistry* **42,** 14814–14821
39. Barth, A., and Zscherp, C. (2002) What vibrations tell us about proteins. *Q. Rev. Biophys.* **35,** 369–430
40. Hellwig, P., Mogi, T., Tomson, F. L., Gennis, R. B., Iwata, J., Miyoshi, H., and Mäntele, W. (1999) Vibrational modes of ubiquinone in cytochrome $bo_3$ from *Escherichia coli* identified by Fourier transform infrared difference spectroscopy and specific $^{13}C$ labeling. *Biochemistry* **38,** 14683–14689
41. Breton, J., Burie, J. R., Berthomieu, C., Berger, G., and Nabedryk, E. (1994) The binding sites of quinones in photosynthetic bacterial reac-

tion centers investigated by light-induced FTIR difference spectroscopy: assignment of the $Q_A$ vibrations in *Rhodobacter sphaeroides* using $^{18}O$- or $^{13}C$-labeled ubiquinone and vitamin $K_1$. *Biochemistry* **33,** 4953–4965

42. Rahmelow, K., Hübner, W., and Ackermann, T. (1998) Infrared absorbances of protein side chains. *Anal. Biochem.* **257,** 1–11
43. Yoshikawa, K., Nakayama, Y., Hayashi, M., Unemoto, T., and Mochida, K. (1999) Koromicin, an antibiotic specific for Gram-negative marine bacteria, strongly inhibits the respiratory chain-linked $Na^+$-translocating NADH:quinone reductase from the marine *Vibrio alginolyticus*. *J. Antibiot.* **52,** 182–185
44. Friedrich, T., Ohnishi, T., Forche, E., Kunze, B., Jansen, R., Trowitzsch, W., Höfle, G., Reichenbach, H., Weiss, H. (1994) Two binding sites for naturally occurring inhibitors in mitochondrial and bacterial NADH: ubiquinone oxidoreductase (complex I). *Biochem. Soc. Trans.* **22,** 226–230